University of Reading

Low-level jets over Utö, Finland, based on Doppler Lidar observations

Article

Published Version

Tuononen, M., O'Connor, E. J., Sinclair, V. A. and Vakkari, V. (2017) Low-level jets over Utö, Finland, based on Doppler Lidar observations. Journal of Applied Meteorology and Climatology, 56 (9). pp. 2577-2594. ISSN 1558-8432 doi: 10.1175/jamc-d-16-0411.1 Available at https://centaur.reading.ac.uk/72707/

It is advisable to refer to the publisher's version if you intend to cite from the work. See Guidance on citing.

To link to this article DOI: http://dx.doi.org/10.1175/jamc-d-16-0411.1

Publisher: American Meteorological Society

All outputs in CentAUR are protected by Intellectual Property Rights law, including copyright law. Copyright and IPR is retained by the creators or other copyright holders. Terms and conditions for use of this material are defined in the End User Agreement.

www.reading.ac.uk/centaur

CentAUR

University of Reading

Central Archive at the University of Reading

Reading's research outputs online

Low-Level Jets over Utö, Finland, Based on Doppler Lidar Observations

MINTTU TUONONEN

Finnish Meteorological Institute, Helsinki, Vaisala Oyj, Vantaa, and Department of Physics, University of Helsinki, Helsinki, Finland

EWAN J. O'CONNOR

Finnish Meteorological Institute, Helsinki, Finland, and Meteorology Department, University of Reading, Reading, United Kingdom

VICTORIA A. SINCLAIR

Department of Physics, University of Helsinki, Helsinki, Finland

VILLE VAKKARI

Finnish Meteorological Institute, Helsinki, Finland

(Manuscript received 16 December 2016, in final form 16 June 2017)

ABSTRACT

Over two years of meteorological observations from Utö, a small island in the Finnish outer archipelago in the Baltic Sea, were used to investigate the occurrence and characteristics of low-level jets (LLJs) and the diurnal and seasonal variations in these properties. An objective LLJ identification algorithm that is suitable for high-temporal-and-vertical-resolution Doppler lidar data was created and applied to wind profiles obtained from a combination of Doppler lidar data and two-dimensional sonic anemometer observations. This algorithm was designed to identify coherent LLJ structures and requires that they persist for at least 1 h. The long-term mean LLJ frequency of occurrence at Utö was 12%, the mean LLJ wind speed was 11.6 m s^{-1}, and the vast majority of identified LLJs occurred below 150 m above ground level. The LLJ frequency of occurrence was much higher during summer (21%) and spring (18%) than in autumn (8%) and winter (3%). During winter and spring, the LLJ frequency of occurrence is evenly distributed throughout the day. In contrast, the LLJ frequency of occurrence peaks at night (1900–0100 UTC) during summer and during the evening hours (1700–1900 UTC) in autumn. The highest and strongest LLJs come from the southwest, which is also the predominant LLJ direction in all seasons. LLJs below 100 m are common in spring and summer, are weaker, and do not show a strong directional dependence.

1. Introduction

Here we define a low-level jet (LLJ) to be a localized maximum in the vertical profile of the horizontal wind that is usually observed in the lowest few hundred meters of the atmosphere. LLJs can be produced by a range of different mechanisms, and the characteristics of LLJs can vary considerably. In this study, a ''climatology'' of LLJs at Utö, a small island in the Finnish archipelago (Fig. 1), is created that incorporates both the frequency of occurrence and the characteristics of all LLJs, regardless of their forcing mechanism.

LLJs have been shown to transport moisture considerable horizontal distances and consequently to influence precipitation patterns and the hydrological cycle (e.g., Higgins et al. 1997). Likewise, pollutants can also be transported horizontally by LLJs, affecting air quality (Mao and Talbot 2004; Hu et al. 2013) and Su et al. (2016) showed that shear-driven turbulence associated with LLJs can transport aerosol and water vapor vertically, influencing cloud formation. Strong shear-driven turbulence below the jet can also have an effect on the surface fluxes of heat and moisture (Banta et al. 2002).

Corresponding author: Minttu Tuononen, minttu.tuononen@fmi.fi

DOI: 10.1175/JAMC-D-16-0411.1

© 2017 American Meteorological Society. For information regarding reuse of this content and general copyright information, consult the AMS Copyright Policy (www.ametsoc.org/PUBSReuseLicenses).

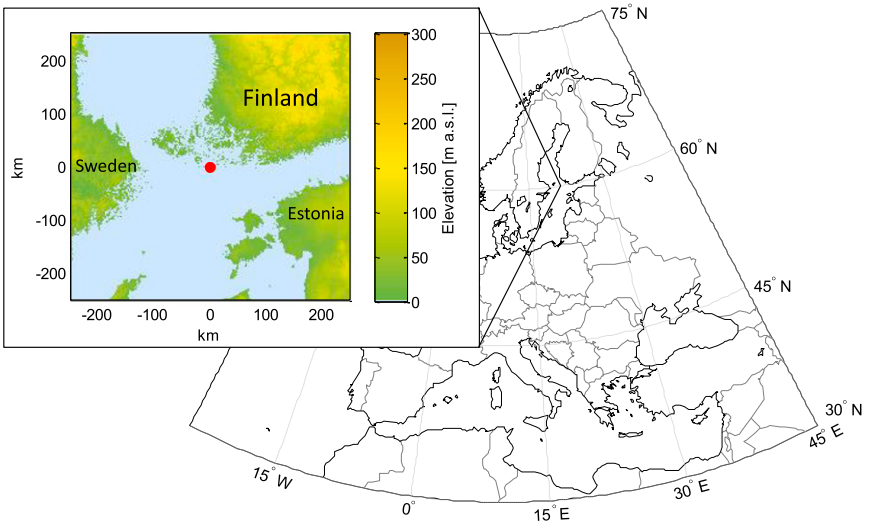

FIG. 1. Location of the Utö measurement site in the Finnish archipelago area. In the 500 km × 500 km topographic map insert for Utö (USGS 2010), the location of the measurement site is indicated by a red dot.

The recent increase in the number of installed wind turbines has also raised interest in LLJs: for example, in the Great Plains and Midwest of the United States (Banta et al. 2006, 2013; Storm et al. 2009; Storm and Basu 2010; Vanderwende et al. 2015), at onshore coastal sites in Denmark (Floors et al. 2013; Peña et al. 2016), and in offshore regions in the Gulf of Maine (Pichugina et al. 2012) and the Baltic Sea (Dörenkämper et al. 2015). Increased shear and associated turbulence related to LLJs are harmful for wind turbines and lower turbine lifetimes (Kelley et al. 2006), but the enhanced low-level wind speeds in the rotor sweep area are potentially beneficial for wind-power production. Therefore, accurate information about how frequently LLJs occur at a specific location, together with the characteristics of the LLJs, would be valuable when planning new wind farms (Kelley et al. 2006).

The occurrence, forcing mechanisms, and impacts of LLJs have been extensively studied over the past 50 years. It is now known that LLJs can develop via inertial oscillations in time (e.g., Blackadar 1957; Mitchell et al. 1995; Baas et al. 2009), large-scale baroclinicity (e.g., Kotroni and Lagouvardos 1993; Whiteman et al. 1997), coastal effects (e.g., Parish 2000; Ranjha et al. 2013; Orr et al. 2005), katabatic winds (e.g., Renfrew and Anderson 2006), and barrier winds (e.g., Parish 1982). Only a brief review of previous LLJ studies and LLJ forcing mechanisms is given here [see Stensrud (1996) and references within for a more complete overview].

The majority of the early observational LLJ studies took place in the United States. For example, Bonner (1968) analyzed observations from 47 rawinsonde stations and determined that LLJs most frequently occurred in the Great Plains. Numerous further studies (e.g., Mitchell et al. 1995; Whiteman et al. 1997) then analyzed the structure and forcing mechanisms for the LLJs that develop in the Great Plains; Mitchell et al. (1995) concluded that the strongest LLJs occurred near local midnight and that a diurnal oscillation in the wind speed and direction was present, indicating that inertial oscillations in time play an important role in the dynamics of these LLJs. These observations supported the theory of inertial oscillations in time proposed by Blackadar (1957). The acceleration of the horizontal wind speed occurs after sunset when the boundary layer undergoes a transition from a well-mixed state to a stably stratified state. The rapid decrease in convectively driven turbulent mixing and, as a consequence, the decay of friction disrupts the force balance among the pressure gradient force, the Coriolis force, and friction, which results in acceleration of the horizontal wind speed in the decoupled boundary layer. Extensive field campaigns have more recently taken place in the Great Plains region and have resulted in extensive knowledge of these nocturnal LLJs (e.g., Banta et al. 2006). Nocturnal LLJs forced by inertial oscillations in time have also been studied in Australia (May 1995) and in the Netherlands (e.g., Baas et al. 2009, 2012).

In comparison with in the United States, fewer LLJ studies, whether focusing on their climatological characteristics or on their forcing mechanisms, have taken place in northern Europe where our study is focused; as a consequence, less is known about LLJs in this region. In addition, many of the studies that have

examined LLJs in the Baltic Sea area have concluded that, unlike in the Great Plains area, LLJs are not predominantly forced by inertial oscillations in time. Högström and Smedman-Högström (1984), Smedman et al. (1993), and Smedman et al. (1995) investigated LLJs, their turbulent characteristics, and forcing mechanisms over the Baltic Sea during spring and summer. They concluded that LLJs occur frequently over the Baltic Sea in the warm season and that they are the result of an "inertial oscillation in space," which is triggered by frictional decoupling at a coastline when relatively warm air passing over a nearby landmass flows out over much colder water. Such LLJs have also been identified elsewhere and are discussed in theoretical studies. Owinoh et al. (2005) and Orr et al. (2005) refer to these LLJs as thermal boundary layer jets and noted the similarity between these and the more classical nocturnal jet forced by temporal, rather than spatial, variations in atmospheric stability. When LLJs are generated by an upwind coastline, however, the acceleration of the wind speed depends on the horizontal distance from the step change in boundary layer stratification, and thus these LLJs usually have no diurnal cycle and cannot be identified from hodographs created from point observations of wind speed and direction. A step change in surface friction can also trigger the development of LLJs—for example, at a coastline when the wind flows from over rough land to smooth sea; such jets are referred to as frictional–Coriolis–buoyancy jets by Orr et al. (2005). More recent studies of LLJs in the Baltic Sea include Dörenkämper et al. (2015), who developed an LLJ climatology by using data from a 100-m mast in the central western Baltic Sea; they concluded that LLJs are most common in spring and least common in winter. In a modeling study, Svensson et al. (2016) showed that LLJs are common over the Baltic Sea and occur at lower heights (210–250 m) in spring than in winter (typically around 450 m).

Many early studies on LLJs analyzed rawinsonde observations (Bonner 1968; Whiteman et al. 1997). The advantages of such observations are their continuous nature (no data gaps) and their vertical extent. Disadvantages are primarily low temporal resolution—for example, Bonner (1968) based his study on twice-daily observations—and the limited number of observing stations. Studies have also analyzed LLJs using meteorological towers or masts (e.g., Dörenkämper et al. 2015), which tend to have good temporal and vertical resolution but are limited to the lowest 100–300 m of the atmosphere.

Remote sensing instruments have much better temporal resolution in comparison with radiosonde observations and provide vertical profiles that extend much farther into the troposphere in comparison with meteorological masts. As a consequence, active remote sensing instruments have been used considerably in more recent LLJ studies. For example, multiple years of wind profiler data were utilized by May (1995) and Song et al. (2005), and Baas et al. (2009) combined 7 years of meteorological mast and wind profiler observations at Cabauw in the Netherlands. Sodar data have also been used to determine the occurrence and characteristics of LLJs—for example, in Florida (Karipot et al. 2009) and in Moscow (Kallistratova and Kouznetsov 2012). High-resolution Doppler lidar has proven to be an ideal instrument to measure vertical wind profiles (Banta et al. 2002, 2013), and Doppler lidar systems have even been deployed on ships (Tucker et al. 2010; Pichugina et al. 2012), enabling the investigation of LLJs in marine locations.

Many of these remote sensing studies have been conducted using research instruments. Although such research instruments clearly provide high-quality observations, it appears to be common to deploy them on short-term field campaigns rather than to operate them at the same location for multiple years at a time. In our study, we use a Doppler lidar that is part of the Finnish Meteorological Institute (FMI) operational ground-based remote sensing network (Hirsikko et al. 2014), the main purpose of which is to monitor winds, air pollution, and boundary layer properties in near–real time. Hence, this Doppler lidar provides a long time series of observations but has a scan strategy that is not optimized for identifying LLJs.

The first aim of this study is to create an objective LLJ identification algorithm. Many previous LLJ studies have developed automated algorithms to identify LLJs from a range of datasets, and we build on these earlier studies (Bonner 1968; Whiteman et al. 1997; Baas et al. 2009; Tuononen et al. 2015). The algorithm developed in this study differs somewhat from earlier algorithms, because it is specifically designed to identify LLJs from high-temporal-and-vertical-resolution operational Doppler lidar data obtained in the particularly clean environment of Utö (the strength of the Doppler lidar signal depends on the scattering from aerosol particles; a clean atmosphere may have too few aerosol particles present to provide sufficient signal). The second aim is to investigate the occurrence and diurnal and seasonal variability of LLJs as well as the LLJ characteristics at Utö, which may be a potential area for future production of wind power.

The paper is structured as follows: A description of the measurement site and lidar observations is given in section 2. The LLJ identification algorithm is discussed

in detail in section 3. Section 4 includes the results of the LLJ occurrence and characteristics at Utö as well as information on the dependence of these results on thresholds applied in the LLJ detection algorithm. In section 5, a brief comparison of our results with earlier studies in the Baltic Sea is given. An optimal scanning scheme for LLJ identification is discussed in section 6, before the conclusions are presented in section 7.

2. Observations

a. Measurement station and data period

Utö is a small, flat island in the Finnish outer archipelago (59.78°N, 21.37°E), located about 80 km from the southwestern tip of the Finnish mainland (Fig. 1). The total area of the island is 0.81 km^2, with the highest point less than 20 m above mean sea level (MSL). Utö is the southernmost island of the Finnish archipelago. To the north, between Utö and the Finnish mainland, there are many islands; to the south the Baltic Sea opens out (Fig. 1). Utö is not located close to the mainland coastlines of Finland, Estonia, or Sweden.

Solar noon at Utö is UTC + 1.4 h. During summer months, the earliest sunrise is at 0413 local time and the latest sunset is at 2300 local time. In contrast, in winter, sunrise is around 0930 and the sun sets around 1530 local time. The lowest monthly mean temperature, −2.2°C, is observed in February, and the highest monthly mean temperature, +16.7°C, is observed in July (Pirinen et al. 2012).

Vertical profiles of horizontal wind obtained from a scanning Doppler lidar were the primary data used for this study, supplemented with two-dimensional (2D) sonic anemometer observations from a nearby tower. Data for this study were gathered quasi continuously from 1 January 2013 to 4 May 2015, with 118 days of data missing because of maintenance and other issues, mostly during spring/summer 2014. Sea ice was not observed near Utö during this study except for a short period in early 2013. The highest sea ice concentrations were observed between 25 February and 14 April 2013, but the Doppler lidar was not operating between 8 March and 5 April 2013.

b. Doppler lidar observations

Vertical profiles of horizontal wind speed and direction were obtained from a Halo Photonics Stream Line Doppler lidar operating routinely as part of the FMI Doppler lidar network (Hirsikko et al. 2014). This instrument operates at a wavelength of 1.5 μm and uses the heterodyne technique to detect the Doppler shift. The pulse repetition frequency was 15 kHz, pulse length was 200 ns, and line-of-sight resolution was 30 m. A total of 320 range gates gives a potential range of 9.6 km, but useful signals are typically limited to much closer ranges because of insufficient numbers of aerosol or cloud particles in the atmosphere. Liquid clouds are excellent targets, but, because they also strongly attenuate the lidar signal, those signals are limited to cloud base and do not penetrate more than a few hundred meters into the cloud. The instrument provides profiles of signal-to-noise ratio and radial Doppler velocity at a user-selected temporal resolution. Postprocessing then applies background corrections to the signal-to-noise ratio (Manninen et al. 2016), and uncertainty estimates for the radial Doppler velocities are obtained directly from the corrected signal-to-noise ratio by using an approximation to the Cramér–Rao lower-bound method (Rye and Hardesty 1993) given in O'Connor et al. (2010). Unreliable radial Doppler velocities are identified by applying the standard operational signal-to-noise ratio threshold of −21 dB; that is, each radial velocity measurement with a signal-to-noise ratio of less than −21 dB has an intrinsic measurement uncertainty of $>0.15\ m\ s^{-1}$ and is discarded.

The Doppler lidar was deployed at 3 m above ground level (AGL) (8 m MSL) and was configured with a scan schedule that included wind scans interspersed with vertical stare and other scans. The wind scans were composed of a Doppler beam swing (DBS) scan and a low-level velocity–azimuth display (VAD) scan (Fig. 2a). The three-beam DBS scan was performed every 10 min and consisted of one beam pointing toward vertical and two orthogonal beams at 70° elevation (from horizontal) (Fig. 2a). The low-level VAD scan was performed every 30 min at 4° elevation and contained 24 beams (one every 15° in azimuth) (Fig. 2a). All wind scans were obtained with a large number of accumulated pulses per beam (>75 000) to ensure high accuracy. One low-level VAD scan takes 2 min to complete, and one three-beam DBS scan takes 1 min. Together with other scans, this leaves about 45 min per hour for vertically pointing operation (Fig. 2c). It is important to note that the instrument scanning schedule that was implemented was designed for other operational requirements and has not been optimized for LLJ studies.

c. Deriving vertical profiles of the horizontal wind

The horizontal wind speed and direction are obtained from DBS (Henderson et al. 2005; Lane et al. 2013) and VAD (e.g., Päschke et al. 2015) scans by using trigonometry and assuming that no major changes occur within the scanning volume (Fig. 2b). Uncertainties in the derived horizontal wind speed and direction are then obtained through propagation of the radial Doppler

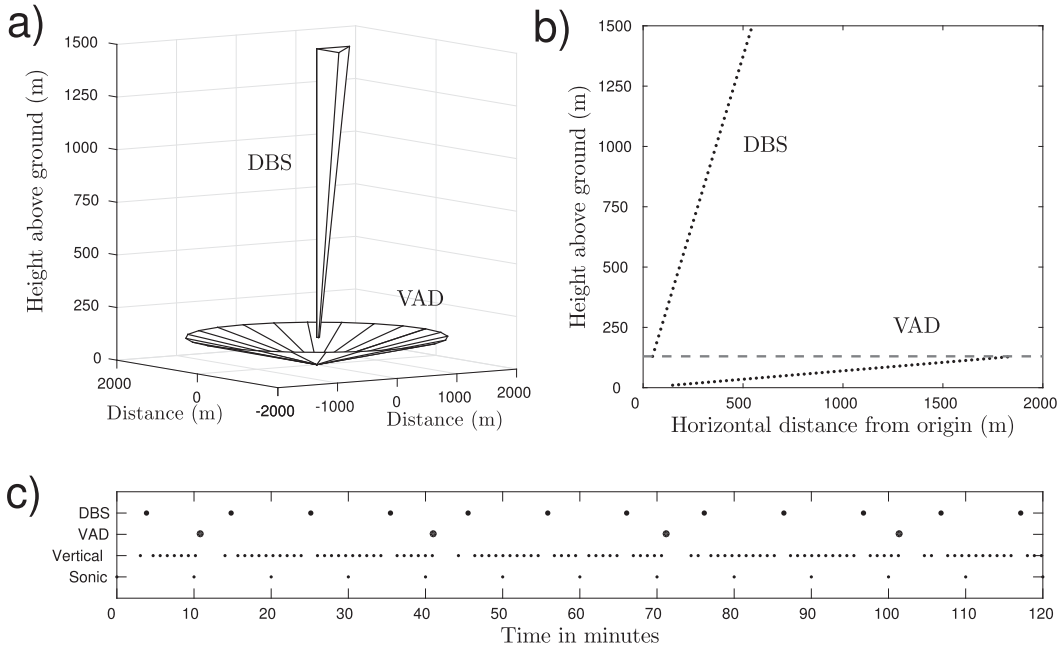

FIG. 2. A schematic drawing that describes scan sequence and scans that are concatenated to create the wind-profile dataset. (a) Illustration of the two Doppler lidar scanning patterns used in this study. Point (0, 0, 0) represents the measurement site. (b) Horizontal and vertical distance from origin for each off-zenith beam from VAD (below 130 m AGL) and DBS (above 130 m AGL) scans. The horizontal dashed line indicates the height level at which the scan pattern used changes from VAD to DBS (at 130 m AGL). (c) Measurement interval for each dataset (DBS scan, VAD scan, vertically pointing operation, and sonic anemometer) used in this study during a 2-h sample period, indicating the effective temporal resolution of each dataset.

velocity uncertainty estimates (e.g., Päschke et al. 2015). Both DBS and VAD methods for obtaining winds assume horizontal homogeneity and stationarity in the wind field, which may not be appropriate in highly turbulent situations (Koscielny et al. 1984). The VAD method proposed by Päschke et al. (2015) uses a quality metric that is based on the coefficient of determination for the sine fit, together with an estimate of the collinearity of the data, to determine reliable data. Such a metric is not available for winds derived from DBS scans, and therefore we use the standard deviation σ_w of the vertical wind to diagnose the presence of turbulence that is sufficient to bias the DBS measurements. The σ_w is calculated from the vertically pointing data from before and after the DBS scan, using a sliding window of 30 min and three range gates centered on each height in the wind profile to ensure a sufficient number of samples for a reliable estimate. The threshold value for σ_w above which wind profiles were discarded for being unreliable was empirically determined to be 0.20 m s^{-1}. Similar values for estimating turbulent situations by Doppler lidar have been used, for example, in Hogan et al. (2009) and Tucker et al. (2009).

The full vertical profile of the horizontal wind is then obtained by concatenating the wind profiles provided by both VAD and DBS Doppler lidar scans. At 2-km radius, the VAD scan at an elevation of 4° from horizontal reaches an altitude of 140 m. Since the maximum range of the VAD scan was typically less than 2 km, we create the concatenated wind profile by limiting the VAD scan to 130 m AGL and then stacking the DBS scan (from 130 m AGL) on top of the VAD scan (Figs. 2a,b). Thus, the lowest measurement height that we use from the low-level VAD scan is 10.3 m AGL, which corresponds to a radius of 148 m, and the lowest height for the DBS scan is 130 m AGL, at which height the off-zenith beams have a horizontal distance of 47 m from the instrument (Fig. 2b). Ten-minute-averaged winds from the 2D sonic anemometer at 20 m AGL were inserted into the concatenated profile at the appropriate height level, and the VAD and 2D sonic anemometer data were interpolated in time to match the DBS time series (data every 10 min).

d. Data availability and quality

The VAD scan is often limited to ranges that are much closer than 2 km because of low aerosol concentrations or intervening cloud and precipitation, and this situation means that there can be gaps in the concatenated wind profile between the highest altitude available from the VAD scan and the first measurement

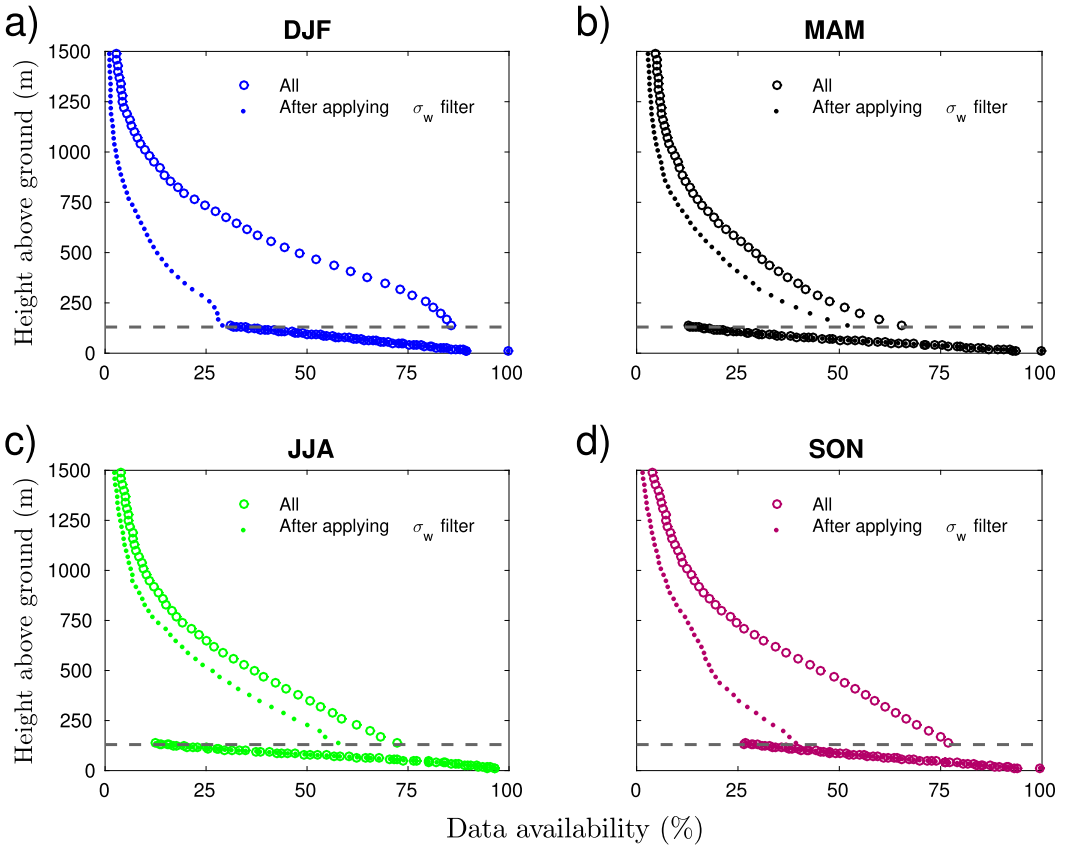

FIG. 3. Concatenated wind-profile data availability vs height above ground for each season: (a) December–February (DJF), (b) March–May (MAM), (c) June–August (JJA) and (d) September–November (SON), before and after applying the σ_w threshold to discard unreliable turbulent wind measurements. Data availability represents the percentage of valid data at each height relative to the total number of observations. Altitudes below 130 m AGL correspond to VAD (and 2D sonic anemometer) data availability; altitudes above 130 m AGL correspond to DBS data availability. The horizontal dashed line indicates the height level at which the scan pattern that is used changes from VAD to DBS (at 130 m AGL).

altitude from the DBS scan. The seasonal data availability for the combined dataset is presented in Fig. 3 and clearly shows the challenge of obtaining signal in a clean atmosphere with a shallow boundary layer. Data availability decreases with range in all seasons, as expected, for both DBS and VAD scans. Clearly visible in Fig. 3 is the considerable impact that applying the σ_w threshold has on DBS data availability, with up to 70% of DBS data with good signal being discarded in winter and 27% being discarded in summer. That turbulent conditions can reduce the number of reliable wind profiles in good signal conditions was also noted by Päschke et al. (2015). Data availability before applying the σ_w threshold was higher in winter and autumn, whereas after applying the σ_w threshold the data availability was lowest in winter. Very few turbulent issues were noted in the VAD scans—a fact that was attributed to the low elevation of the scanning angle. We do not expect LLJs to be present during strong convectively driven turbulent conditions, however, and therefore the discarding of a significant portion of the DBS data should not affect the true LLJ climatology. The potential impact of the data availability on the LLJ climatology is discussed in section 3.

It is clear that the 4°-elevation VAD scan, 70°-elevation DBS scan, and 2D sonic anemometer are not measuring the same volume, with each measurement type representing different atmospheric scales. For example, at 127 m in altitude the VAD scan radius is 1.8 km, whereas at 130 m in altitude the horizontal distance for the off-zenith DBS beams is 47 m (Fig. 2b). To check whether this method of creating a concatenated wind profile was valid, in Fig. 4a the winds obtained from the 2D sonic anemometer were compared with the VAD winds closest to the anemometer height. In addition, in Fig. 4b the wind speed from the lowest DBS height (130 m AGL) was

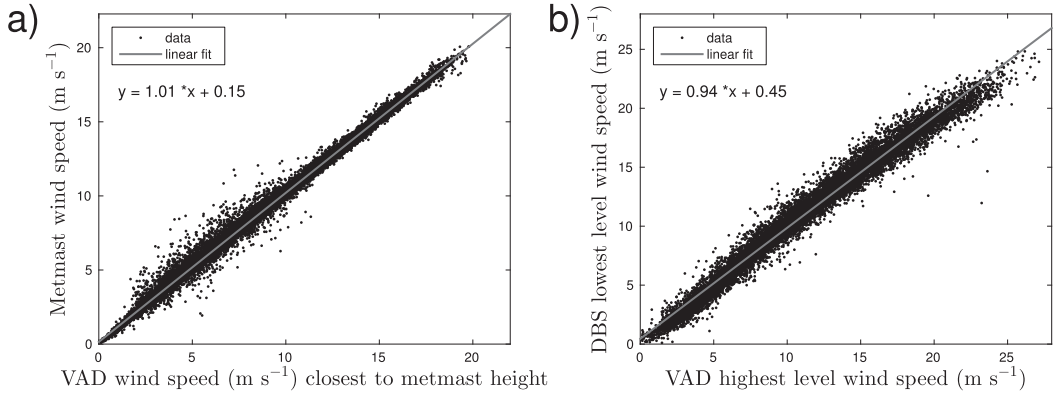

FIG. 4. (a) Comparison of 2D sonic anemometer wind speed from the meteorological mast (at 20 m AGL) and Doppler lidar VAD wind speed from the height that is closest to that 2D sonic anemometer measurement height (21 m AGL), and (b) comparison of Doppler lidar DBS wind speed at the lowest available level (130 m AGL) and Doppler lidar VAD wind speed at the highest level that was used (128 m).

compared with the wind speed from the closest VAD range gate to this height (128 m AGL). Both comparisons showed minimal bias, with a root-mean-square error for the VAD–DBS comparison of $0.87\,\mathrm{m\,s^{-1}}$ and a root-mean-square error of $0.29\,\mathrm{m\,s^{-1}}$ for the VAD–2D sonic anemometer comparison. These values give us confidence that, at this location and despite the differences in the measurement volumes, the method used to obtain a concatenated wind profile is suitable for diagnosing LLJs.

3. Low-level-jet identification algorithm

The LLJ identification algorithm consists of two parts, 1) main criteria and 2) threshold criteria, that were applied to the quality-controlled concatenated wind-profile data. The main criteria are used to find all low-level wind speed maxima in each wind profile. The threshold criteria result in coherent LLJ cases, without sudden jumps in LLJ height, wind speed, and wind direction, and ignore individual wind speed maxima that should not be identified as LLJ cases. The algorithm logic is as follows.

For each wind profile, all local wind speed maxima and minima below 1510 m are identified. After finding all local maxima and minima, the main criteria are applied to each wind profile that contains at least one local maximum: if a local maximum is both at least $2\,\mathrm{m\,s^{-1}}$ stronger and at least 25% stronger than the local minima below and above the local maximum, the local maximum will be denoted as a low-level wind speed maximum. The main criteria are checked for all local maxima in each profile. Up to three low-level wind speed maxima are permitted in each individual wind profile, allowing multiple LLJs, at different heights, to be identified within a single profile.

After finding all low-level wind speed maxima, the threshold criteria are applied. An individual profile with at least one low-level wind speed maximum that meets all of the thresholds is then designated as an LLJ profile. One LLJ case is defined to be a quasi-continuous time series of LLJ profiles, and therefore every LLJ profile belongs to an LLJ case. The threshold criteria ensure that an LLJ case consists of LLJ profiles that have similar characteristics and thus are coherent features without any large or sudden changes in height, speed, or direction. It also allows short time gaps in the data. All subjectively chosen thresholds (labeled 1–4 below) are checked simultaneously and must be fulfilled as follows:

1) The height difference (Δh in Fig. 5a) between two consecutive low-level wind speed maxima must be smaller than 135 m. This absolute threshold value corresponds to the height of four range gates in the Doppler lidar DBS data.
2) The wind speed difference (Δws in Fig. 5b) between two consecutive low-level wind speed maxima must be smaller than 30%. This relative value allows larger absolute differences when the wind speed is high and smaller absolute differences with low wind speed.
3) The wind direction difference (Δwd in Fig. 5c) between two consecutive low-level wind speed maxima must be smaller than 45°.
4) The time difference (Δt in Fig. 5d) between two consecutive low-level wind speed maxima must be smaller than 1 h. This absolute value will allow some missing wind profiles (i.e., data gaps) between two consecutive LLJ profiles in the same LLJ case.

If any one of the thresholds 1–4 described above is not fulfilled, the low-level wind speed maximum being

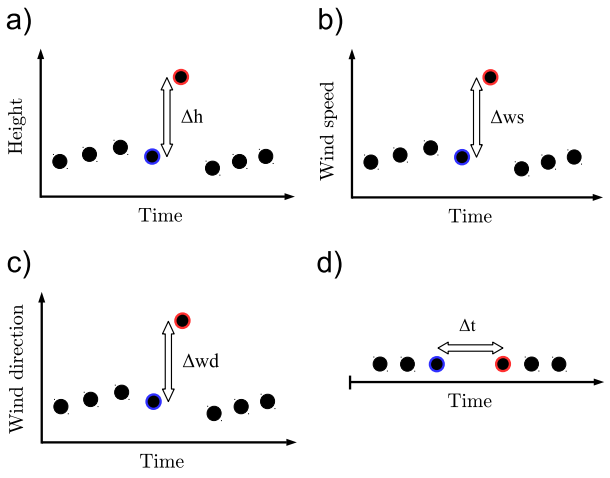

FIG. 5. A schematic drawing that describes the different threshold criteria used for identifying LLJ profiles on the basis of (a) height, (b) wind speed, (c) wind direction, and (d) time differences between two consecutive low-level wind speed maxima (Δh, Δws, Δwd, and Δt, respectively). Filled black circles represent low-level wind speed maxima fulfilling the main criteria described in section 3. Each low-level wind speed maximum (e.g., red-edged profile) is compared with the previous low-level wind speed maximum (blue-edged profile) and differences (Δh, Δws, Δwd, and Δt) between these consecutive low-level wind speed maxima are tested against the threshold values simultaneously. If any difference values (Δh, Δws, Δwd, or Δt) between two consecutive low-level wind speed maxima are larger than the given threshold value, the low-level wind speed maximum does not belong to the same LLJ case as the previous LLJ profile.

tested does not belong to the same LLJ case as the earlier low-level wind speed maxima that fulfilled the criteria. Furthermore, the low-level wind speed maximum that did not fulfill the threshold criteria is not rejected until it is verified that it is not the initial low-level wind speed maximum of a new LLJ case. Each LLJ case is labeled with a running number, and therefore it is possible to calculate the estimate of the duration of each LLJ case. In addition, it is required that each LLJ case must last at least 1 h; this ensures that only coherent LLJ structures are detected and prevents isolated individual profiles that happen to meet the rest of the criteria from being identified as an LLJ case.

The principles behind the main criteria are very similar to those presented in previous studies. The LLJ criteria used by Bonner (1968) and Whiteman et al. (1997) used stricter thresholds for the LLJ maximum and falloff above the maximum; however, these studies did not test for a minimum below the maximum. In contrast, the algorithm by Banta et al. (2002) consisted of looser absolute thresholds for LLJ maximum and falloffs for the minima, both below and above the maximum. Andreas et al. (2000) used an absolute criterion that was similar to that used in this study, but they did not use a relative falloff criterion for the minima. The main criteria are also similar to those applied by Baas et al. (2009) and Tuononen et al. (2015), consisting of both absolute and relative criteria with similar magnitudes. High temporal resolution permits testing the persistence of the LLJ, with a requirement that is similar to that imposed by Baas et al. (2009). The additional threshold criteria employed here have been designed specifically for high-resolution Doppler lidar data to enable the identification of coherent LLJ cases rather than individual LLJ profiles.

On applying the main and threshold criteria to strict quality-controlled Doppler lidar wind-profile data, it can be seen that the algorithm is capable of objectively identifying LLJ cases (Fig. 6). In some situations in which the air is very clean or clouds are present, the Doppler lidar signal is too weak and therefore wind measurements, especially at higher altitudes in the atmosphere, are missing. Missing data are shown in white in Fig. 6, and there is often a small gap in the concatenated profile after combining the VAD and DBS scans, as seen around the heights below 200 m in Fig. 6. This occurs because there is not enough signal in the VAD scan at far ranges, as shown in the data-availability plot (Fig. 3). Data gaps may also exist as a result of the instrument conducting other scan types as part of its operational routine. The algorithm detects an LLJ case when all criteria are fulfilled but may discard some viable cases as a result of data gaps even though the LLJ likely continues during the data gap. Such cases are potentially visible in Fig. 6b. An LLJ is detected at 0000 UTC 17 May 2013 and continues until 0500 UTC 17 May 2013, but, between 0500 and 1100 UTC 17 May 2013, there are no data available above 100 m AGL and, therefore, no LLJ is identified by the algorithm, even though it is likely that the LLJ persisted through this period. A similar situation also occurs in the evening between 1630 and 2100 UTC 17 May. Because of data limitations, such as operational data gaps and inability to observe the entire wind profile in all weather situations with the Doppler lidar (such as in the presence of low clouds), the LLJ duration calculation is only suggestive and should be taken as a lower limit. How data limitations and data availability can affect the LLJ statistics presented here is also discussed in section 4.

4. LLJ characteristics over Utö, Finland

a. *LLJ frequency of occurrence*

On the basis of more than 2 years of Doppler lidar data, the LLJ frequency of occurrence at Utö is 12%, calculated by dividing all identified LLJ profiles by the number of observed wind profiles. At Utö, LLJs are more common

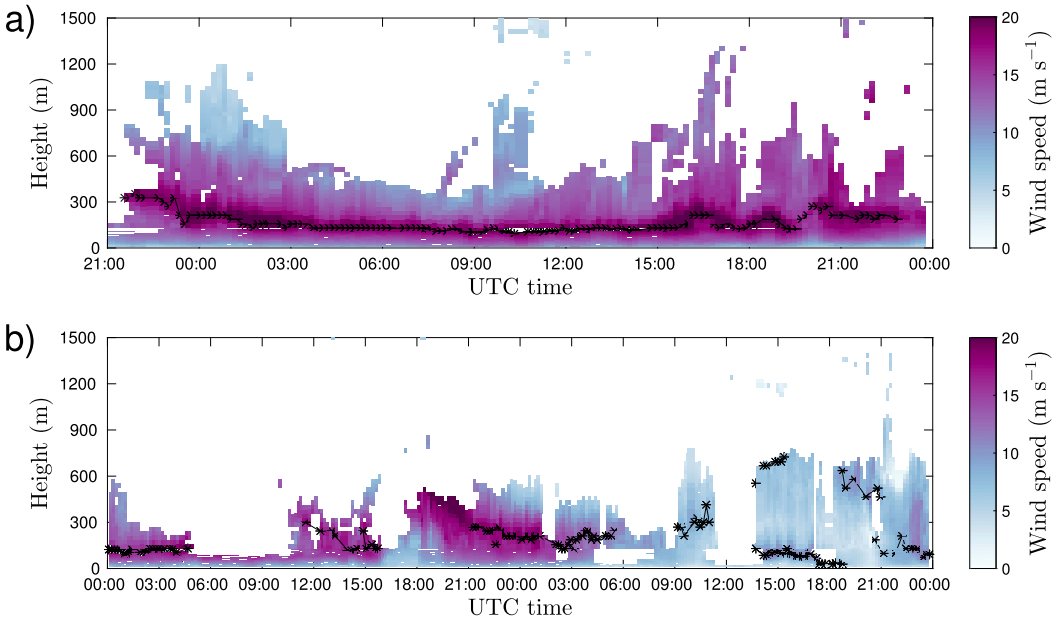

FIG. 6. Time–height plots of horizontal wind speed derived from Doppler lidar data at Utö (a) between 2100 UTC 20 May 2013 and 0000 UTC 22 May 2013 and (b) between 17 and 18 May 2013. Horizontal wind speed is given by the color shades; white regions denote missing wind speed data due to lack of signal. Black stars denote LLJ profiles, with black lines linking appropriate LLJ profiles into an LLJ case.

during spring and summer than in winter and autumn (Fig. 7a); the LLJ frequency of occurrence is highest between March and August and is lowest between November and February, with a maximum in July (28%) and a minimum in December (2%). The values of LLJ frequency of occurrence corresponding to each month, season, or hour are normalized by the number of wind profiles measured during each month, season, or hour. Therefore, the values of LLJ frequency of occurrence account for the variation in the number of observed wind profiles. Multiple LLJs (i.e., more than one low-level wind speed maximum belonging to separate LLJ cases in one wind profile) were found in 0.1% of all wind profiles, corresponding to 1% of all LLJ profiles.

There is little diurnal variation in LLJ frequency of occurrence during winter and spring (Fig. 7b), but the mean LLJ frequency of occurrence is 15% higher in spring than in winter. Some diurnal variation is present during summer, with LLJ frequency of occurrence enhanced at night, by up to 15%, and in autumn, when LLJs are up to 8% more common in the early evening. Note that all values of LLJ frequency of occurrence should be considered as a lower bound because of the data limitations, as discussed in section 3.

b. *LLJ characteristics*

The LLJ height (Table 1) is usually lowest in summer (median LLJ height 104 m) and highest in winter (median LLJ height 243 m). Figure 8a shows the distribution of LLJ heights observed in each season. The vast majority of LLJs identified are below 200 m, with a peak occurrence observed between 130 and 200 m. The observed LLJ height distribution in spring is very similar to that of summer, with low (below 100 m) LLJs being common. During autumn, there are more LLJs at higher levels and, similar to what is observed in winter, far fewer LLJs identified below 100 m. Figure 8a shows that many LLJs occur between 130 and 200 m, corresponding to the three lowest DBS levels, but, in reality, the true wind maximum may occur slightly below 130 m. This is a consequence of the low VAD data availability at far ranges (Fig. 3) relative to the DBS data availability at near ranges; the LLJ maximum is likely to be observed at the first available DBS range gates (from 130 m AGL above) in which there is much more signal. There is a larger jump in data availability between the farthest VAD range and the first DBS range in spring and summer (Figs. 3b,c), which may explain the strong peak in LLJ occurrence at the lowest DBS levels in spring and summer. Thus, interpreting the distribution of LLJ height should be made in reference to the data availability at each height.

The mean LLJ wind speed is 11.6 m s^{-1} (standard deviation of 4.3 m s^{-1}) with a median value of 10.8 m s^{-1}, a result of a slightly positively skewed LLJ wind speed distribution (Table 1). The median wind speeds in autumn

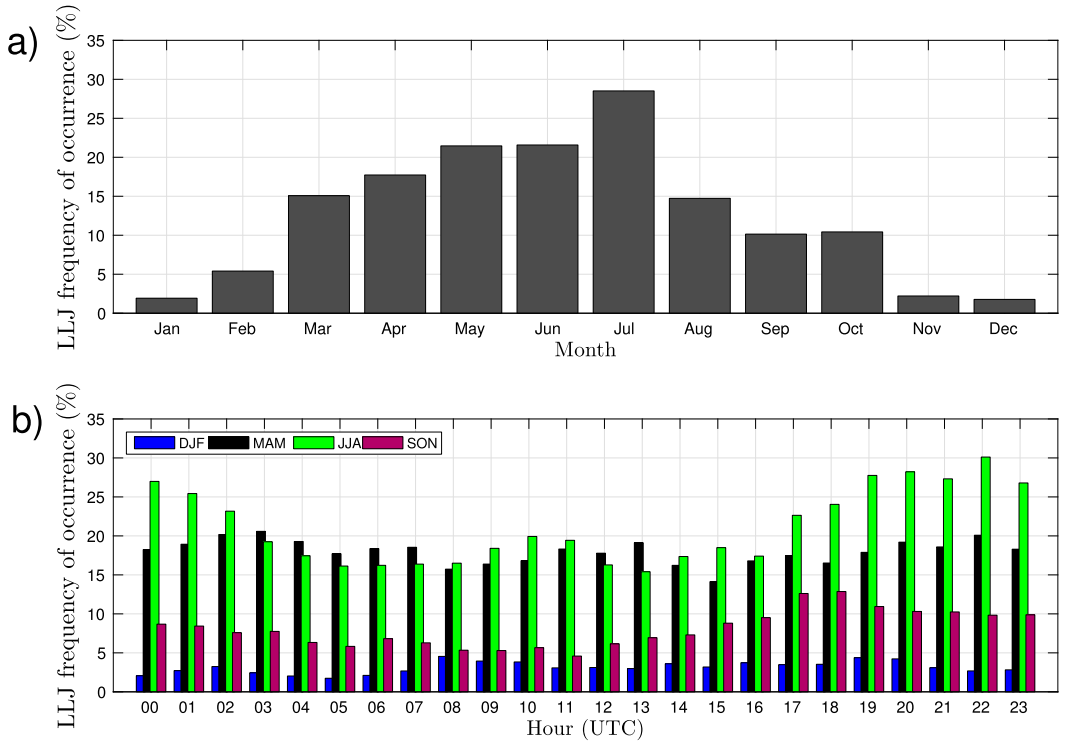

FIG. 7. Histograms that show (a) monthly variation of LLJ frequency of occurrence and (b) hourly variation of LLJ frequency of occurrence, separated by season. Each bar is normalized by the number of wind profiles of the corresponding month or hour.

($10.0\,\mathrm{m\,s^{-1}}$) and in summer ($10.6\,\mathrm{m\,s^{-1}}$) are weaker than in winter ($11.8\,\mathrm{m\,s^{-1}}$) and in spring ($11.4\,\mathrm{m\,s^{-1}}$). The LLJ wind speed distribution also varies from season to season (Fig. 8b), with a narrow distribution in summer and broader distributions with longer tails toward stronger wind speeds during other seasons. The wintertime distribution is particularly broad.

Three wind directions dominate LLJ occurrence over Utö: 1) east–east-southeast, 2) south-southwest–west, and 3) north–northwest (Fig. 8c). All three directions are well represented during spring and summer months, whereas during winter months the dominant LLJ direction is from the south-southwest. In autumn, the most common direction for LLJ occurrence is from the southwesterly sector, together with a slight increase in LLJ occurrence from the southeast.

The LLJ bulk speed shears below and above the LLJ are respectively defined as

$$\alpha_{\mathrm{below}} = \frac{U_{\mathrm{LLJ}} - U_{\mathrm{min,below}}}{h_{\mathrm{LLJ}} - h_{\mathrm{min,below}}} \quad \text{and} \tag{1}$$

$$\alpha_{\mathrm{above}} = \frac{U_{\mathrm{min,above}} - U_{\mathrm{LLJ}}}{h_{\mathrm{min,above}} - h_{\mathrm{LLJ}}}, \tag{2}$$

where U_{LLJ} is the LLJ wind speed, $U_{\mathrm{min,below}}$ and $U_{\mathrm{min,above}}$ are respectively the wind speeds of the minima below and above the LLJ, h_{LLJ} is the LLJ height, and $h_{\mathrm{min,below}}$ and $h_{\mathrm{min,above}}$ are respectively the heights of the minima below and above the jet. Median values of bulk speed shear above and below the jet are -0.019 and $0.048\,\mathrm{m\,s^{-1}\,m^{-1}}$ (Table 1), respectively, and the distributions of LLJ bulk speed shear values below the jet are much broader than the distributions of shear values above the jet. These observations demonstrate that the speed shear is, in most cases, stronger below the LLJ than above it. This usually is because most LLJs are very low in altitude (below 150 m) and, therefore, the height difference $h_{\mathrm{LLJ}} - h_{\mathrm{min,below}}$ in Eq. (1) is usually smaller than the height difference $h_{\mathrm{min,above}} - h_{\mathrm{LLJ}}$ in Eq. (2).

The mean and median bulk speed shear above and below the LLJ are strongest in spring (median values are $-0.022\,\mathrm{m\,s^{-1}\,m^{-1}}$ above and $0.057\,\mathrm{m\,s^{-1}\,m^{-1}}$ below) and weakest in winter (median values are $-0.013\,\mathrm{m\,s^{-1}\,m^{-1}}$ above and $0.028\,\mathrm{m\,s^{-1}\,m^{-1}}$ below). Above the jet, the distribution of speed shear values is similar for all seasons, peaking between -0.01 and $-0.02\,\mathrm{m\,s^{-1}\,m^{-1}}$. In contrast, below the jet, in winter and autumn the distributions are more positively skewed than in spring and summer, denoting larger shear values during spring and

TABLE 1. LLJ statistics showing mean, 25th, 50th (median), and 75th percentiles of LLJ height, LLJ wind speed, and bulk speed shears above and below the LLJ on each season.

	Season	Mean	25th percentile	Median	75th percentile
LLJ height (m)	All	161	81	121	158
	Winter	254	130	243	327
	Spring	141	75	113	158
	Summer	140	73	104	130
	Autumn	206	109	130	271
LLJ wind speed ($m\,s^{-1}$)	All	11.6	8.7	10.8	13.7
	Winter	12.5	9.3	11.8	15.6
	Spring	12.2	8.9	11.4	14.8
	Summer	10.9	8.7	10.6	12.7
	Autumn	11.5	8.0	10.0	13.0
Speed shear above the LLJ ($s^{-1}\,m^{-1}$)	All	−0.024	−0.030	−0.019	−0.011
	Winter	−0.016	−0.019	−0.013	−0.009
	Spring	−0.028	−0.034	−0.022	−0.013
	Summer	−0.024	−0.030	−0.020	−0.012
	Autumn	−0.020	−0.024	−0.015	−0.008
Speed shear below the LLJ ($s^{-1}\,m^{-1}$)	All	0.054	0.031	0.048	0.071
	Winter	0.030	0.017	0.028	0.040
	Spring	0.063	0.040	0.057	0.082
	Summer	0.058	0.036	0.052	0.077
	Autumn	0.035	0.022	0.031	0.046

summer below the jet. Eight percent of bulk speed shear values are larger than $0.1\,m\,s^{-1}\,m^{-1}$, and 1% are smaller than $-0.1\,m\,s^{-1}\,m^{-1}$.

Figures 9a–d show how the LLJ height varies with speed and direction during each season. The highest and strongest LLJs typically arrive from southwesterly directions, which is also the prevailing wind direction at this site. These LLJs occur in all seasons. Other strong and high LLJs arrive from the east and from the north-northwest; these are present in spring and summer, with the easterly LLJs being slightly stronger and higher. LLJs at heights below 100 m have low wind speeds (typically $<15\,m\,s^{-1}$) and appear to be evenly distributed in all directions, except in winter.

c. *Threshold sensitivity in the LLJ identification algorithm*

In comparison with previous automated LLJ identification algorithms that were predominantly applied to observations with coarser temporal resolution by, for example, Bonner (1968), Whiteman et al. (1997), and Baas et al. (2009) and to gridded reanalysis data by, for example, Rife et al. (2010), Ranjha et al. (2013), and Tuononen et al. (2015), our newly developed algorithm includes some extra subjectively chosen thresholds and criteria. To ensure that the results presented here are not strongly threshold dependent, in this section we analyze the impact of all thresholds that were applied.

The sensitivity of the LLJ characteristics—that is, LLJ frequency of occurrence (Fig. 10a), LLJ mean height (Fig. 10b), LLJ mean speed (Fig. 10c), number of LLJ cases (Fig. 10d), and LLJ duration (Fig. 10e)—to the threshold values used in the LLJ identification algorithm was analyzed by changing one threshold value at a time while keeping the others constant (the default values are those described in section 3). Threshold values for the change in the height, speed, and direction between two consecutive low-level wind speed maxima (e.g., as described in Figs. 5a–c) were varied by ±10%, ±30%, ±50%, and ±70% relative to the default thresholds. Furthermore, the accepted time difference between two consecutive low-level wind speed maxima (as described in Fig. 5d) was also varied by ±10%, ±30%, ±50%, and ±70% relative to the default threshold. Last, the sensitivity to the duration criterion—that is, how long an LLJ case needs to be—was investigated by varying the default value by ±10%, ±30%, ±50%, and ±70%. Note that, except in the case of the duration threshold, when the threshold values are decreased the algorithm becomes stricter and when they are increased the algorithm becomes less stringent.

The LLJ frequency of occurrence is the most sensitive to the time-difference threshold between two consecutive low-level wind speed maxima (Fig. 10a). When the time-difference threshold is changed by −70% (equivalent to setting it to be less than 18 min), the LLJ frequency of occurrence decreases to 7%. Changes in the other thresholds do not affect the LLJ frequency of occurrence as much, especially when the algorithm is relaxed. By changing any threshold by ±30%, the LLJ

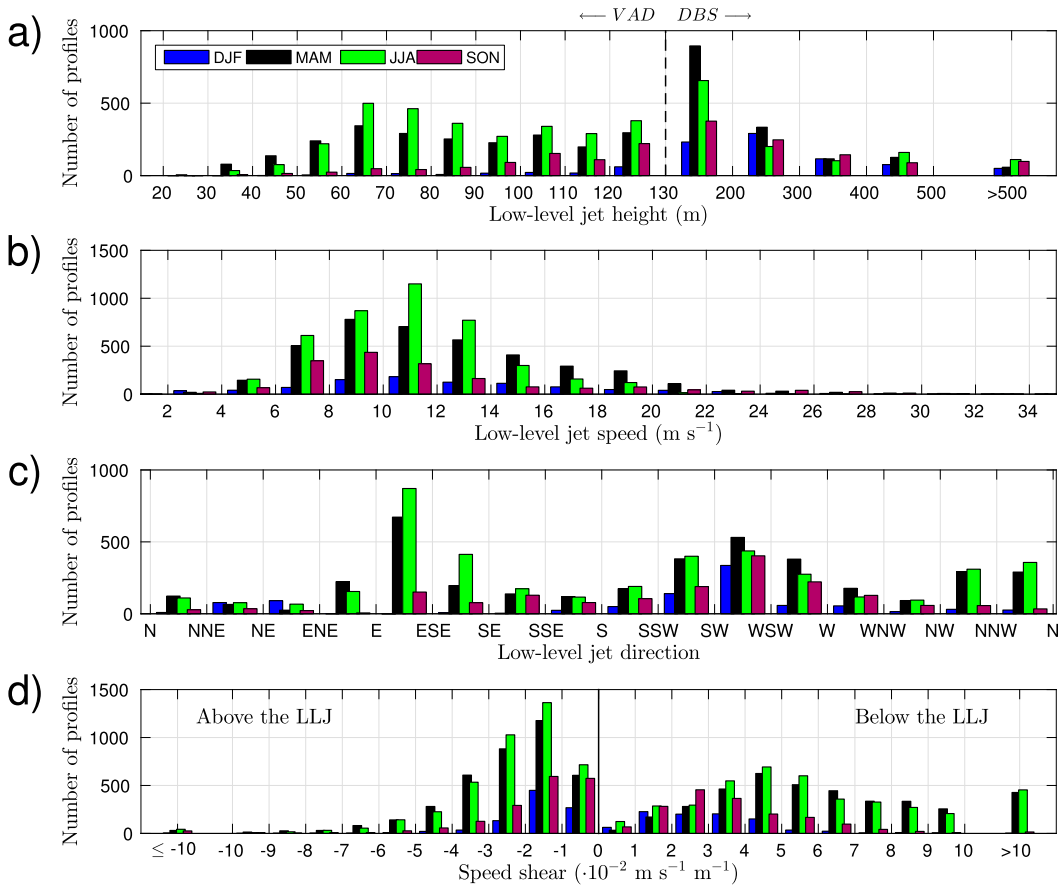

FIG. 8. Histograms that show (a) LLJ height (note the unequal bin edges on the x axis, corresponding to 4–5 gates in the VAD range and 3–4 gates in the DBS range, except the last bin), (b) LLJ speed, (c) LLJ direction, and (d) LLJ bulk speed shear (by definition: <0 above the LLJ and >0 below the LLJ). Each bar represents the number of profiles between the tick values. Results are separated by different seasons.

frequency of occurrence changes by less than ±1% relative to the LLJ frequency of occurrence as calculated with the default thresholds.

The LLJ mean height is affected most when the height-difference threshold or time-difference threshold between two consecutive low-level wind speed maxima is changed (Fig. 10b). The duration threshold also affects the mean LLJ height but in the opposite direction. This result is consistent with expectations, because the longer cases usually occur at lower heights. For any threshold change of ±30% or less, however, the LLJ mean height varies by less than 20 m, which is smaller than the vertical resolution of the data obtained from the DBS scans.

The impact on LLJ mean speed is marginal for any threshold variation up to ±70% (Fig. 10c), especially for any increase in threshold value. Even when the thresholds are decreased by 70%, the resulting LLJ mean speed varies by less than 0.6 m s^{-1}, and the extreme values are within ±1% relative to the reference mean LLJ speed.

The number of LLJ cases is mostly affected by changing the time threshold and the duration threshold (Fig. 10d), as expected. If the time gap between two low-level wind speed maxima is less than 18 min (70% decrease relative to the reference time-difference threshold), the number of LLJ cases clearly decreases. In contrast, by requiring the LLJ duration to be only 18 min, the number of LLJ cases clearly increases. Because the percentage change in the number of cases is much larger than for any other LLJ statistic, we conclude that, of all of the LLJ statistics that we consider, the number of LLJ cases is most susceptible to the subjective threshold choice and is the least reliable.

The LLJ duration is affected mostly when the duration threshold or the time threshold is changed. If the time threshold is reduced (allowing a shorter time gap between two consecutive low-level wind speed maxima), the algorithm splits LLJ cases more often into shorter cases. In contrast, allowing a longer time gap allows LLJ cases to continue across missing data.

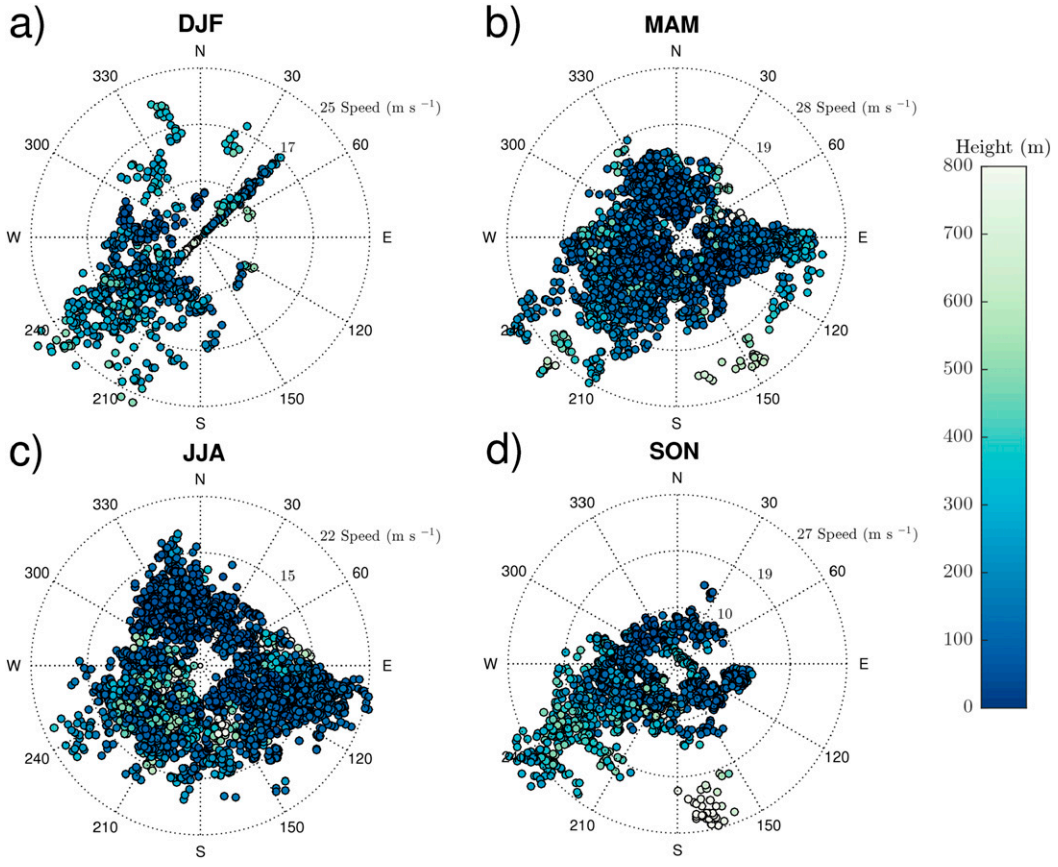

FIG. 9. Scatterplots that show how LLJ height varies with LLJ speed and direction for each season: (a) DJF, (b) MAM, (c) JJA, and (d) SON. LLJ speed and direction are presented in polar coordinates, and the color of the circle shows the LLJ height. Values for each individual LLJ profile within all observed LLJ cases are plotted. Note that each plot has a different scaling for the LLJ wind speed. LLJ direction is defined as the direction from which the wind is coming.

However, increasing the allowed time gap also permits the algorithm to combine cases that do not have the same characteristics and therefore should not be identified as the same case (not shown). Other thresholds have a minimal effect on the mean LLJ duration.

Overall, changing the duration threshold has the largest effect on the results, especially in the mean height, number of cases, and LLJ duration itself. If the LLJ duration threshold is increased, the mean LLJ height is lower, the number of LLJs is decreased, and the duration is longer relative to the reference. On the contrary, if shorter LLJs are allowed, the mean height is higher, the number of LLJs is larger, and the duration is shorter relative to the reference. The length of the allowed time gap between two consecutive low-level wind speed maxima also affects the results. Both of these thresholds are essential for the algorithm to operate because of the characteristics of the Doppler lidar data that are available at this location (described in section 3), and the reference values for these thresholds were selected on the basis of the time resolution and limitations of the data. Otherwise, the observed LLJ characteristics are not sensitive to the choice of threshold if it is within ±30% of the reference thresholds employed in this study.

5. Comparison with earlier studies in the Baltic Sea

We now compare the results presented here with previous studies that were conducted close to Utö. Quantitative comparison is often difficult because of the differences in the measurement period, LLJ identification criteria, instrument capabilities, and data resolution.

Dörenkämper et al. (2015) investigated the seasonal variation of LLJ occurrence and LLJ characteristics in the western Baltic Sea (55.00°N, 13.15°E) on the basis of 6 years of mast measurements up to 102 m MSL. They define an LLJ event such that the wind speed at any altitude below 102 m must exceed the wind speed measured at 102 m by a certain percentage value

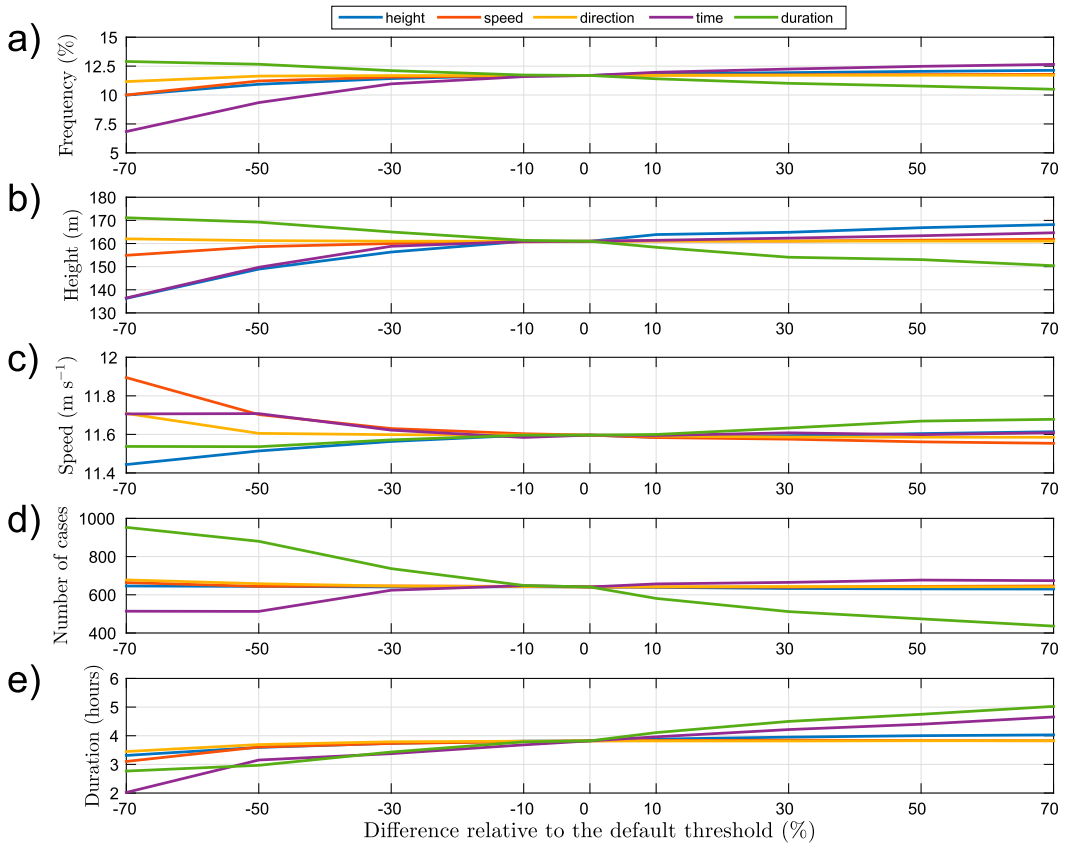

FIG. 10. Sensitivity of (a) LLJ frequency of occurrence, (b) mean LLJ height, (c) mean LLJ speed, (d) number of LLJ cases, and (e) mean LLJ duration to the different thresholds that are used in the LLJ identification algorithm described in section 3 and shown in Fig. 5. The corresponding lines and thresholds are given by blue for the height threshold, orange for the speed threshold, yellow for the direction threshold, purple for the time threshold, and green for the duration threshold.

(10%, 20%, 30%, or 40%). Dörenkämper et al. (2015) found the highest LLJ occurrence in spring (7% with the least-strict criteria) and the lowest occurrence in winter (<1% with the least-strict criteria). They found no strong diurnal cycle for springtime LLJs but slightly enhanced LLJ occurrence in summer evenings. Our results show enhanced LLJ occurrence throughout the night in summer, whereas in autumn increased LLJ frequency of occurrence is found in the evening. Our results show higher LLJ frequency of occurrences, and, in contrast to the study by Dörenkämper et al. (2015), the highest LLJ frequency of occurrence is found in summer (21%) and the second highest is found in spring (18%). Differences between the results may be due to the different vertical extent of the two different measurement systems (meteorological mast vs Doppler lidar) and consequently the different definitions of an LLJ. Although both sites were located in the Baltic Sea, the different site characteristics may also play a role.

To enable a fairer comparison with the results of Dörenkämper et al. (2015), our statistics were recalculated by limiting the results to LLJ maxima identified below 102 m MSL. The observed diurnal cycle of LLJ occurrence in these recalculated statistics is similar to that found by Dörenkämper et al. (2015) both in spring and summer (not shown). In addition, the LLJ frequency of occurrence at Utö decreases to 10% in summer and 7% in spring and similarly is low in winter (0.2%) and autumn (1.2%). These recalculated statistics compare better to the study by Dörenkämper et al. (2015); note, however, that, although we consider only LLJs below 102 m, the minimum above the jet is usually found above 102 m.

Högström and Smedman-Högström (1984), and Smedman et al. (1993, 1995) investigated LLJs in the Baltic coast of Sweden and the Stockholm archipelago on the basis of double-theodolite pilot-balloon measurements, radiosoundings, aircraft measurements, and modeling. They found spring- and summertime LLJs

that were forced by an inertial oscillation in space in situations in which the flow is directed from a warmer coast (Swedish or Latvian coast) over the colder Baltic Sea. According to Smedman et al. (1995), summertime LLJs—observed by the radiosonde observations and modeled by the numerical simulations in the Stockholm archipelago, and forced by an inertial oscillation in space—occur at low altitudes (30–100 m) and reach speeds of 12 m s^{-1}. In addition, on the basis of idealized 2D-modeling experiments, Savijärvi (2011) found summertime LLJs along the southern coast of Finland that were due to inertial oscillations in space when the flow was directed from the Estonian coast over the colder sea. Furthermore, the model results by Savijärvi (2011) revealed easterly LLJs with height and speed characteristics that were similar to those reported here in Doppler lidar data from Utö.

It is also interesting to compare our observations with results that were obtained from a reanalysis dataset. Wintertime (October–March) LLJs were diagnosed from the ''Arctic system reanalysis'' (ASR) for the period of 2000–10 by Tuononen et al. (2015). They found that the wintertime LLJ frequency of occurrence at the grid point nearest to Utö was 18%, with an LLJ mean height of 340 m and an LLJ mean wind speed of 11 m s^{-1}. These LLJs were higher and weaker than those observed with the Doppler lidar, probably as a result of both the coarser vertical resolution close to the ground in ASR and the reduction in data availability at higher altitudes in the observations. This would also explain why there are more LLJs diagnosed in ASR than in the observations. The predominant LLJ direction in ASR was from the west, with the majority occurring within the west-to-south sectors; our observations show southwest as the predominant LLJ direction. Although progress has been made in representing LLJs in high-resolution numerical models (e.g., Hu et al. 2013; Vanderwende et al. 2015), this comparison suggests that deficiencies are still evident in coarser-vertical-resolution reanalysis datasets, especially when attempting to diagnose LLJs below 100 m.

6. Optimizing scanning for LLJs

It is clear that the scanning scheme employed at this location is not optimal for diagnosing LLJs, especially because it necessitates combining two scan types with very different data availabilities at the height at which they are stacked (130 m). Although LLJs are not expected in strong convectively driven turbulent conditions, such conditions do affect the wind retrievals, with DBS scans suffering strongly from violation of the homogeneity assumption necessary for the retrieval. VAD scans mitigate this impact, but VADs are also susceptible to turbulence causing the homogeneity assumption to be violated, especially at higher scan elevations (Päschke et al. 2015). Therefore, an ideal scan strategy would involve the use of one VAD scan at an elevation that gives full coverage through the extent of the boundary layer (i.e., up to at least 1.5 km in altitude) while still providing sufficient vertical resolution near the surface to enable the calculation of both the LLJ maximum and the minimum below for LLJs below 100 m. A suitable elevation angle for the scan will depend on the range resolution of the instrument that is performing the scans. An instrument with a radial range resolution of 100 m must scan lower than an instrument with a radial range resolution of 30 m to obtain the same vertical resolution; an elevation angle of 9° for a range resolution of 100 m and 30° for a range resolution of 30 m will permit a vertical resolution of 15 m.

Our results indicate that the temporal resolution of the scans (10 min for DBS; 30 min for VAD) was sufficient for capturing LLJs so that when selecting an integration time the focus should be on obtaining high-quality data rather than rapid scans (i.e., taking 4 min to complete one high-quality VAD scan may be preferable to a sequence of 10 scans taking 24 s each). The integration time will depend on location since it depends on the amount of aerosol that is present in the atmosphere.

7. Conclusions

An LLJ identification algorithm was developed specifically for objective identification of LLJs in Doppler lidar data with high temporal and vertical resolution. The algorithm was applied to more than 2 years of Doppler lidar data from Utö, an island in the Finnish outer archipelago, to determine the LLJ frequency of occurrence, the statistics of LLJ characteristics, and their seasonal and diurnal variability. In the future, this algorithm can easily be applied to data from different locations and even in an operational context. In this study, the wind profiles, used as input to the LLJ identification algorithm, are obtained by combining observations from two different Doppler lidar scanning patterns (DBS and VAD) with additional anemometer wind data. In addition, a data-quality step was applied, removing measurements for which the homogeneity assumption was unlikely to be satisfied because of the presence of convectively driven turbulence.

LLJs were identified in 12% of all observed wind profiles at Utö. The vast majority of LLJs were identified below 150 m AGL, and the mean LLJ wind speed was 11.6 m s^{-1}. The LLJ frequency of occurrence should be considered as a lower limit because of data limitations.

For example, some LLJs may be missed because of data gaps that can occur during cloudy conditions or when the air is very clean—a more common problem in Utö than in most European locations—because the lidar signal is too weak. Low data availability at higher altitudes as a result of the lack of signal limits any detection of potential LLJs at these altitudes, directly affecting our results. The data availability below 400 m AGL, however, was sufficient to capture LLJs that can have an impact on wind energy, which was one motivation of this study.

The LLJ frequency of occurrence was higher during spring and summer (up to 30% during summer nights) than in autumn and was lowest in winter (<5% throughout the day). During summer, LLJs occur at lower heights and are slightly weaker than they are in other seasons. The highest and strongest LLJs come from the southwest, which is also the predominant LLJ direction in all seasons. Other common directions in spring and summer are east and north-northwest, which exhibit lower and slightly weaker LLJs. LLJs below 100 m are the weakest, show little directional dependence, and are most common in spring and summer.

We have shown that LLJ is a common phenomenon and occurs at relatively low altitudes at Utö, especially during the spring and summer seasons. Since LLJs can have a positive impact on the production of wind power and a potential negative impact on the lifetime and efficiency of wind turbines (Kelley et al. 2006), the ability to provide long-term climatological descriptions of LLJ characteristics is crucial when considering future increases in offshore wind-turbine installations in the Finnish archipelago. Numerical models are used to provide wind-resource assessments for wind-energy purposes, and these observations will be used to evaluate whether such models are capable of producing LLJs accurately in this region. In addition, the characteristics of the shear-driven turbulence associated with LLJs, which were not included in this study, should be examined in detail to understand their impact on wind-turbine stress and wind-power production. The objective algorithm created for this study can be used to identify LLJs operationally, verify numerical model output, and guide decision-making regarding wind-power installations in the future.

Acknowledgments. Author MT was supported by the Maj and Tor Nessling Foundation (Grants 201500300 and 201600003). Author VAS was funded by the Academy of Finland (Project 3073314). We also acknowledge the support from EU COST Action ES1303 TOPROF.

REFERENCES

Andreas, E. L, K. J. Claffy, and A. P. Makshtas, 2000: Low-level atmospheric jets and inversions over the western Weddell Sea. *Bound.-Layer Meteor.*, **97**, 459–486, doi:10.1023/A:1002793831076.

Baas, P., F. C. Bosveld, H. K. Baltink, and A. A. M. Holtslag, 2009: A climatology of nocturnal low-level jets at Cabauw. *J. Appl. Meteor. Climatol.*, **48**, 1627–1642, doi:10.1175/2009JAMC1965.1.

——, B. J. H. van de Wiel, L. van den Brink, and A. Holtslag, 2012: Composite hodographs and inertial oscillations in the nocturnal boundary layer. *Quart. J. Roy. Meteor. Soc.*, **138**, 528–535, doi:10.1002/qj.941.

Banta, R. M., R. K. Newsom, J. K. Lundquist, Y. L. Pichugina, R. L. Coulter, and L. Mahrt, 2002: Nocturnal low-level jet characteristics over Kansas during CASES-99. *Bound.-Layer Meteor.*, **105**, 221–252, doi:10.1023/A:1019992330866.

——, Y. L. Pichugina, and W. A. Brewer, 2006: Turbulent velocity-variance profiles in the stable boundary layer generated by a nocturnal low-level jet. *J. Atmos. Sci.*, **63**, 2700–2719, doi:10.1175/JAS3776.1.

——, ——, N. D. Kelley, R. M. Hardesty, and W. A. Brewer, 2013: Wind energy meteorology: Insight into wind properties in the turbine-rotor layer of the atmosphere from high-resolution Doppler lidar. *Bull. Amer. Meteor. Soc.*, **94**, 883–902, doi:10.1175/BAMS-D-11-00057.1.

Blackadar, A. K., 1957: Boundary layer wind maxima and their significance for the growth of nocturnal inversions. *Bull. Amer. Meteor. Soc.*, **38**, 283–290.

Bonner, W. D., 1968: Climatology of the low level jet. *Mon. Wea. Rev.*, **96**, 833–850, doi:10.1175/1520-0493(1968)096<0833:COTLLJ>2.0.CO;2.

Dörenkämper, M., M. Optis, A. Monahan, and G. Steinfeld, 2015: On the offshore advection of boundary-layer structures and the influence on offshore wind conditions. *Bound.-Layer Meteor.*, **155**, 459–482, doi:10.1007/s10546-015-0008-x.

Floors, R., C. L. Vincent, S. E. Gryning, A. Peña, and E. Batchvarova, 2013: The wind profile in the coastal boundary layer: Wind lidar measurements and numerical modelling. *Bound.-Layer Meteor.*, **147**, 469–491, doi:10.1007/s10546-012-9791-9.

Henderson, S. W., P. Gatt, D. Rees, and R. M. Huffaker, 2005: Wind lidar. *Laser Remote Sensing*, T. Fujii and T. Fukuchi, Eds., CRC Press, 469–722.

Higgins, R. W., Y. Yao, E. S. Yarosh, J. E. Janowiak, and K. C. Mo, 1997: Influence of the Great Plains low-level jet on summertime precipitation and moisture transport over the central United States. *J. Climate*, **10**, 481–507, doi:10.1175/1520-0442(1997)010<0481:IOTGPL>2.0.CO;2.

Hirsikko, A., and Coauthors, 2014: Observing wind, aerosol particles, cloud and precipitation: Finland's new ground-based remote-sensing network. *Atmos. Meas. Tech.*, **7**, 1351–1375, doi:10.5194/amt-7-1351-2014.

Hogan, R. J., A. L. M. Grant, A. J. Illingworth, G. N. Pearson, and E. J. O'Connor, 2009: Vertical velocity variance and skewness in clear and cloud-topped boundary layers as revealed by Doppler lidar. *Quart. J. Roy. Meteor. Soc.*, **135**, 635–643, doi:10.1002/qj.413.

Högström, U., and A.-S. Smedman-Högström, 1984: The wind regime in coastal areas with special reference to results obtained from the Swedish wind energy program. *Bound.-Layer Meteor.*, **30**, 351–373, doi:10.1007/BF00121961.

Hu, X.-M., P. M. Klein, M. Xue, F. Zhang, D. C. Doughty, R. Forkel, E. Joseph, and J. D. Fuentes, 2013: Impact of the vertical mixing induced by low-level jets on boundary layer ozone concentration. *Atmos. Environ.*, **70**, 123–130, doi:10.1016/j.atmosenv.2012.12.046.

Kallistratova, M. A., and R. D. Kouznetsov, 2012: Low-level jets in the Moscow region in summer and winter observed with a sodar network. *Bound.-Layer Meteor.*, **143**, 159–175, doi:10.1007/s10546-011-9639-8.

Karipot, A., M. Y. Leclerc, and G. Zhang, 2009: Characteristics of nocturnal low-level jets observed in the north Florida area. *Mon. Wea. Rev.*, **137**, 2605–2621, doi:10.1175/2009MWR2705.1.

Kelley, N. D., B. J. Jonkman, and G. N. Scott, 2006: The Great Plains turbulence environment: Its origins, impact and simulation. National Renewable Energy Laboratory Conf. Paper NREL/CP-500-40176, 21 pp, https://www.nrel.gov/docs/fy07osti/40176.pdf.

Koscielny, A. J., R. J. Doviak, and D. S. Zrnic, 1984: An evaluation of the accuracy of some radar wind profiling techniques. *J. Atmos. Oceanic Technol.*, **1**, 309–320, doi:10.1175/1520-0426(1984)001<0309:AEOTAO>2.0.CO;2.

Kotroni, V., and K. Lagouvardos, 1993: Low-level jet streams associated with atmospheric cold fronts: Seven case studies from the Fronts 87 Experiment. *Geophys. Res. Lett.*, **20**, 1371–1374, doi:10.1029/93GL01701.

Lane, S. E., J. F. Barlow, and C. R. Wood, 2013: An assessment of a three-beam Doppler lidar wind profiling method for use in urban areas. *J. Wind Eng. Ind. Aerodyn.*, **119**, 53–59, doi:10.1016/j.jweia.2013.05.010.

Manninen, A. J., E. J. O'Connor, V. Vakkari, and T. Petäjä, 2016: A generalised background correction algorithm for a Halo Doppler lidar and its application to data from Finland. *Atmos. Meas. Tech.*, **9**, 817–827, doi:10.5194/amt-9-817-2016.

Mao, H., and R. Talbot, 2004: Role of meteorological processes in two New England ozone episodes during summer 2001. *J. Geophys. Res.*, **109**, D20305, doi:10.1029/2004JD004850.

May, P. T., 1995: The Australian nocturnal jet and diurnal variations of boundary-layer winds over Mt. Isa in north-eastern Australia. *Quart. J. Roy. Meteor. Soc.*, **121**, 987–1003, doi:10.1002/qj.49712152503.

Mitchell, M. J., R. W. Arritt, and K. Labas, 1995: A climatology of the warm season Great Plains low-level jet using wind profiler observations. *Wea. Forecasting*, **10**, 576–591, doi:10.1175/1520-0434(1995)010<0576:ACOTWS>2.0.CO;2.

O'Connor, E. J., A. J. Illingworth, I. M. Brooks, C. D. Westbrook, R. J. Hogan, F. Davies, and B. J. Brooks, 2010: A method for estimating the turbulent kinetic energy dissipation rate from a vertically pointing Doppler lidar, and independent evaluation from balloon-borne in-situ measurements. *J. Atmos. Oceanic Technol.*, **27**, 1652–1664, doi:10.1175/2010JTECHA1455.1.

Orr, A., J. Hunt, R. Capon, J. Sommeria, D. Cresswell, and A. Owinoh, 2005: Coriolis effects on wind jets and cloudiness along coasts. *Weather*, **60**, 291–299, doi:10.1256/wea.219.04.

Owinoh, A. Z., J. C. R. Hunt, A. Orr, P. Clark, R. Klein, H. J. S. Fernando, and F. T. N. Nieuwstadt, 2005: Effects of changing surface heat fluxes on the atmospheric boundary layer flow over flat terrain. *Bound.-Layer Meteor.*, **116**, 331–361, doi:10.1007/s10546-004-2819-z.

Parish, T. R., 1982: Barrier winds along the Sierra Nevada Mountains. *J. Appl. Meteor.*, **21**, 925–930, doi:10.1175/1520-0450(1982)021<0925:BWATSN>2.0.CO;2.

——, 2000: Forcing of the summertime low-level jet along the California coast. *J. Appl. Meteor.*, **39**, 2421–2433, doi:10.1175/1520-0450(2000)039<2421:FOTSLL>2.0.CO;2.

Päschke, E., R. Leinweber, and V. Lehmann, 2015: An assessment of the performance of a 1.5 μm Doppler lidar for operational vertical wind profiling based on a 1-year trial. *Atmos. Meas. Tech.*, **8**, 2251–2266, doi:10.5194/amt-8-2251-2015.

Peña, A., and Coauthors, 2016: Ten years of boundary-layer and wind-power meteorology at Høvsøre, Denmark. *Bound.-Layer Meteor.*, **158**, 1–26, doi:10.1007/s10546-015-0079-8.

Pichugina, Y. L., R. M. Banta, W. A. Brewer, S. P. Sandberg, and R. M. Hardesty, 2012: Doppler lidar–based wind-profile measurement system for offshore wind-energy and other marine boundary layer applications. *J. Appl. Meteor. Climatol.*, **51**, 327–349, doi:10.1175/JAMC-D-11-040.1.

Pirinen, P., H. Simola, J. Aalto, J.-P. Kaukoranta, P. Karllson, and R. Ruuhela, 2012: Climatological statistics of Finland 1981–2010. Finnish Meteorological Institute Rep. 2012:1, 92 pp.

Ranjha, R., G. Svensson, M. Tjernström, and A. Semedo, 2013: Global distribution and seasonal variability of coastal low-level jets derived from ERA-Interim reanalysis. *Tellus*, **65A**, doi:10.3402/tellusa.v65i0.20412.

Renfrew, I. A., and P. S. Anderson, 2006: Profiles of katabatic flow in summer and winter over Coats Land, Antarctica. *Quart. J. Roy. Meteor. Soc.*, **132**, 779–802, doi:10.1256/qj.05.148.

Rife, D. L., J. O. Pinto, A. J. Monaghan, C. A. Davis, and J. R. Hannan, 2010: Global distribution and characteristics of diurnally varying low-level jets. *J. Climate*, **23**, 5041–5064, doi:10.1175/2010JCLI3514.1.

Rye, B. J., and R. M. Hardesty, 1993: Discrete spectral peak estimation in incoherent backscatter heterodyne lidar. I: Spectral accumulation and the Cramer–Rao lower bound. *IEEE Trans. Geosci. Remote Sens.*, **31**, 16–27, doi:10.1109/36.210440.

Savijärvi, H. I., 2011: Anti-heat island circulations and low-level jets on a sea gulf. *Tellus*, **63A**, 1007–1013, doi:10.1111/j.1600-0870.2011.00531.x.

Smedman, A.-S., M. Tjernström, and U. Högström, 1993: Analysis of the turbulence structure of a marine low-level jet. *Bound.-Layer Meteor.*, **66**, 105–126, doi:10.1007/BF00705462.

——, H. Bergström, and U. Högström, 1995: Spectra, variances and length scales in a marine stable boundary layer dominated by a low level jet. *Bound.-Layer Meteor.*, **76**, 211–232, doi:10.1007/BF00709352.

Song, J., K. Liao, R. L. Coulter, and B. M. Lesht, 2005: Climatology of the low-level jet at the southern Great Plains Atmospheric Boundary Layer Experiments site. *J. Appl. Meteor.*, **44**, 1593–1606, doi:10.1175/JAM2294.1.

Stensrud, D. J., 1996: Importance of low-level jets to climate: A review. *J. Climate*, **9**, 1698–1711, doi:10.1175/1520-0442(1996)009<1698:IOLLJT>2.0.CO;2.

Storm, B., and S. Basu, 2010: The WRF Model forecast-derived low-level wind shear climatology over the United States Great Plains. *Energies*, **3**, 258–276, doi:10.3390/en3020258.

——, J. Dudhia, S. Basu, A. Swift, and I. Giammanco, 2009: Evaluation of the Weather Research and Forecasting Model on forecasting low-level jets: Implications for wind energy. *Wind Energy*, **12**, 81–90, doi:10.1002/we.288.

Su, J., M. Felton, L. Lei, M. P. McCormick, R. Delgado, and A. St. Pé, 2016: Lidar remote sensing of cloud formation caused by low-level jets. *J. Geophys. Res. Atmos.*, **121**, 5904–5911, doi:10.1002/2015JD024590.

Svensson, N., H. Bergström, E. Sahlée, and A. Rutgersson, 2016: Stable atmospheric conditions over the Baltic Sea: Model evaluation and climatology. *Boreal Environ. Res.*, **21**, 387–404.

Tucker, S. C., C. J. Senff, A. M. Weickmann, W. A. Brewer, R. M. Banta, S. P. Sandberg, D. C. Law, and R. M. Hardesty, 2009: Doppler lidar estimation of mixing height using turbulence, shear, and aerosol profiles. *J. Atmos. Oceanic Technol.*, **26**, 673–688, doi:10.1175/2008JTECHA1157.1.

——, and Coauthors, 2010: Relationships of coastal nocturnal boundary layer winds and turbulence to Houston ozone concentrations during TexAQS 2006. *J. Geophys. Res.*, **115**, D10304, doi:10.1029/2009JD013169.

Tuononen, M., V. A. Sinclair, and T. Vihma, 2015: A climatology of low-level jets in the mid-latitudes and polar regions of the Northern Hemisphere. *Atmos. Sci. Lett.*, **16**, 492–499, doi:10.1002/asl.587.

USGS, 2010: Global multi-resolution terrain elevation data. U.S. Geological Survey, accessed 4 March 2015, http://earthexplorer.usgs.gov/.

Vanderwende, B. J., J. K. Lundquist, M. E. Rhodes, E. S. Takle, and S. L. Irvin, 2015: Observing and simulating the summertime low-level jet in central Iowa. *Mon. Wea. Rev.*, **143**, 2319–2336, doi:10.1175/MWR-D-14-00325.1.

Whiteman, C. D., X. Bian, and S. Zhong, 1997: Low-level jet climatology from enhanced rawinsonde observations at a site in the Southern Great Plains. *J. Appl. Meteor.*, **36**, 1363–1376, doi:10.1175/1520-0450(1997)036<1363:LLJCFE>2.0.CO;2.